LA-UR- 08-5114

Approved for public release;
distribution is unlimited.

Title:	Luminescence and Structural Properties of Oxyorthosilicate and Al2O3 Nanophosphors
Author(s):	Michael W. Blair Luiz G. Jacobsohn Bryan L. Bennett Stephanie C. Tornga Eduardo G. Yukihara Ross E. Muenchausen
Intended for:	Physica Status Solidi C

Los Alamos
NATIONAL LABORATORY
EST. 1943

Form 836 (7/06)

pss-Header will be provided by the publisher

Luminescence and structural properties of oxyorthosilicate and Al_2O_3 nanophosphors

Michael W. Blair [*,1], Luiz G. Jacobsohn[1], Bryan L. Bennett[1], Stephanie C. Tornga[1], Eduardo G. Yukihara[2], and Ross E. Muenchausen[1]

[1] Los Alamos National Laboratory, P.O. Box 1663, Los Alamos, NM 87545, USA
[2] Oklahoma State University, Physics Department, 145 PS II, Stillwater, OK 74978, USA

Received zzz, revised zzz, accepted zzz
Published online zzz (Dates will be provided by the publisher.)

PACS 81.40-z, 81.20.Ka, 64.70.Nd, 78.55.-m, 76.30.Kg, 78.60.Kn

* Corresponding author: e-mail mblair@lanl.gov, Phone: +1 505 667 7981, Fax: +1 505 665 3866

A large amount of research has been conducted on semiconducting quantum dots exploring quantum confinement effects. On the other hand, nanophosphors – inorganic insulating nanostructured luminescent materials – have received considerably less attention. Our research involving nanomaterials has then focused on the question: How does reduced dimensionality affect the physical and chemical behaviour of nanophosphors?

In order to partially answer this fundamental question, we have produced numerous oxides, among them Lu2SiO5:Ce (LSO), Y2SiO5:Ce (YSO), Gd2SIO5:Ce (GSO), and Al_2O_3, and characterized their structural and luminescent properties. Structure, grain size, phase purity and chemical homogeneity in the nanoscale were determined using x-ray diffraction, transmission electron microscopy, and electron paramagnetic resonance. The luminescent properties of the nanophosphors were characterized by thermoluminescence, radioluminescence, photoluminescence, and optically stimulated luminescence. In this work, we will present an overview of the nascent field of nanophosphors, and summarize the results obtained in our laboratory with particular emphasis on the luminescent properties.

1 Introduction Nanoscience research in photonics, magnetics, sensors, synthesis, and instrumentation continues to be an exciting and fruitful area of research [1]. Semiconducting materials such as quantum dots, particularly the photonic properties of these materials, have been the primary focus of nanoscience research. Our work has focused on a different class of materials – namely nanostructured insulators or nanophosphors which have remained largely unexplored until recently [2].

Although phosphors play an integral role in numerous aspects of modern life with applications ranging from fluorescent lighting and cathode ray tube displays to medical imaging (i.e., positron emission tomography scanners) [3], we have focused on nanophosphor materials that show promise as nuclear radiation detectors. In these luminescent materials, the electronic and optical properties of the luminescent centres are affected by the local symmetry, crystalline structure, degree of structural disorder, defects and chemical composition. In addition, the presence of other dopants or impurities can alter energy transfer processes. In nanophosphors, myriad surface effects are possible related to structural relaxation, reconstruction, dangling bonds, aging, etc, that arise from the high surface-to-volume ratio of nanoparticles.

In this paper, we first examine rare-earth (RE) doped nanophosphors such as oxyorthosilicates (including Ce-doped Lu_2SiO_5 (LSO), Y_2SiO_5 (YSO), and Gd_2SiO_5 (GSO)) with emphasis on optical properties and how these change with reduced dimensionality. The structural and optical properties of storage nanophosphors (e.g., Al_2O_3) have also been studied as these materials are of utmost importance in passive personal dosimetry.

2 Materials and Methods

2.1 Solution Combustion Synthesis The nanophosphors discussed in this paper were produced by the Solution Combustion Synthesis (SCS) technique [4]. In this process, commercial nanopowders are dissolved in an excess of nitric acid. After the exothermic reaction

cools, the resulting nitrate solutions are divided into crucibles. A measured amount of fuel (either urea, glycine, or hexamethylenetetramine (HMT) for our experiments) is then added and the samples are dried in a vacuum oven at 115 °C for 1 hour. The samples are then combusted in air in a muffle furnace, and the samples are finally annealed at 1000 °C for 1 hour to remove any excess fuel and nitrate residues.

2.2 Characterization techniques Structural and morphological characterization was carried out by a Siemens D5000 x-ray diffractometer with $Cu_{k\alpha}$ radiation, and TEM measurements. Preliminary TEM measurements used a Phillips CM30 microscope operated at 300 kV, while high resolution (HRTEM) and scanning (STEM) TEM used a JEOL 2010F microscope operated at 200 kV

Photoluminescence excitation (PLE) and emission (PL) measurements were obtained in ambient conditions using a Photon Technology International TimeMaster™ fluorimeter.

Radioluminescence (RL) measurements were carried out in vacuum at room temperature using a Mo-target X-ray source operating at 50 kV and 40 mA. The effective X-ray energy was ~25 keV and the dose rate at the sample was 1.75 Gy/s (measured in air).

Thermoluminescence (TL) experiments were carried out on one of two commercial systems. A Harshaw TLD Model 3500 manual reader measured TL (at a heating rate of 5 ^{0}C/s) from sample powders on a silver planchet after they had been exposed to 25 keV X-rays. A Risø TL/OSL DA-15 [5] automated system was also used where powder samples were affixed to stainless steel disks using silicone spray and irradiations were performed with an on-board $^{90}Sr/^{90}Y$ β irradiation source delivering 0.129 Gy/s. The samples were heated at a rate of 1 °C/s and light detection was accomplished via a photomultiplier tube (PMT) with bialkali photocathode (Thorn-EMI 9235QA). The same TL/OSL DA-15 system was used for OSL measurements where 470 nm optical stimulation was provided by a LED array.

Electron paramagnetic resonance (EPR) spectroscopy measurements were made both at room temperature and liquid helium temperature with a Bruker EleXsys E-500 spectrometer equipped with an Oxford cryostat. The X-band spectrometer consists of an SHQE-W1 cavity, SuperX bridge, NMR Tesla meter, and field/frequency stabilizer. Data were acquired by taking the first derivative of the absorption curve with field modulation 100 kHz and amplitude 0.4 mT. Powder samples were placed in a fused silica tube and inserted into the microwave cavity for measurement.

3 Oxyorthosilicates In this paper, we discuss experiments on Ce-doped LSO, YSO, and GSO nanophosphor oxyorthosilicates. The samples were produced by the SCS method using X_2O_3 (where X=Lu, Y, or Gd) as starting materials. After dissolution in nitric acid, $Ce(NO_3)_3 \cdot 6H_2O$ (for Ce doing) and fumed silica were added to the mixture. After combustion and annealing, the process resulted in agglomerated X_2SiO_5:Ce (where again X=Lu, Y, or Gd) nanophosphors.

3.1 Nanophosphor structure

LSO and YSO crystals grown by the Czochralski (CZ) method are known to crystallize in the monoclinic C2/c structure with Lu or Y (and Ce upon doping) occupying two distinct sites with 6 and 7 oxygen coordination respectively. GSO crystals, on the other hand, have $P2_1/c$ symmetry with 7 and 9 oxygen coordination [6]. XRD analysis shows that all of the oxyorthosilicate nanophosphors produced in our lab crystallize in the $P2_1/c$ structure with 7 and 9 oxygen coordination. These results mean that nanostructured LSO and YSO are structurally different from their bulk counterparts while GSO has the same structure for nanophosphor and bulk specimens, and the structural changes will be important when considering changes in luminescence properties.

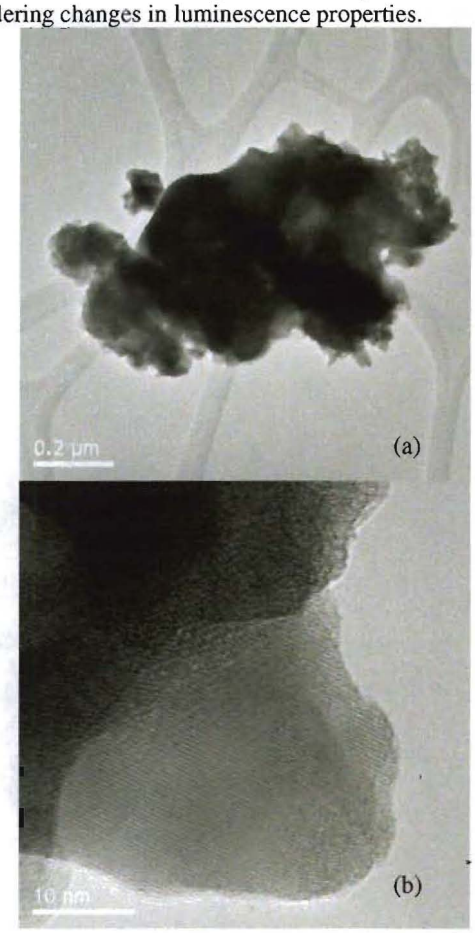

Figure 1 TEM of nanophosphor LSO showing (a) micron sized agglomerated crystallites and (b) a single crystallite.

Nanophosphor oxyorthosilicate microstructure was further investigated through TEM (Fig.1). While the average crystallite size is consistent with the XRD Debye-

Scherrer analysis that yielded 30 nm, TEM analysis revealed a broad size distribution, with dimensions typically ranging from 20 to 80 nm and micron sized agglomerated particles. The crystallites show no evidence of an amorphous core, indicating complete reaction. On the other hand, they have many dislocations and stacking faults, which is not unexpected for combustion produced materials [7]. Electron energy loss spectroscopy (EELS) in conjunction with STEM on Tb-doped nanophosphors has recently confirmed that the dopant is homogenously distributed within the nanophosphor for SCS produced samples [10].

3.2 Luminescence properties

Luminescence results from RL and PL have previously been reported for nanophosphor YSO [9], LSO, and GSO [10]. Surprisingly, the nanophosphor oxyorthosilicates are nominally as bright as their bulk counterparts when stimulated by X radiation (RL) or ultraviolet light (PL). Our experiments have largely centred on trying to understand the increased light output from the nanophosphor oxyorthosilicates and the role of reduced dimensionality.

By comparing the normalized PLE and PL curves for bulk and nanophosphors, it can be seen that n-LSO and n-YSO display approximately 20 nm red shifts and considerably less self-absorption as compared to the bulk specimens. The reduced self-absorption in the nanoparticles could partially explain their increased PL intensities. However, the PL peak shifts are unlikely to be due to reduced dimensionality as n-GSO shows only a 5 nm red shift (as compared to bulk). Since the XRD results showed that n-YSO and n-LSO have different crystal structures from bulk crystals while n-GSO and bulk GSO have the same crystal structure, the changes in PL peak positions can be attributed to changes in the activator ion (e.g., Ce) symmetry [10].

Reduced dimensionality probably plays a more important role in another aspect of nanophosphor luminescence. In CZ grown oxyorthosilicates, the maximum Ce concentration is limited by the low segregation coefficient [11] to about 0.05% and the luminescence intensity as a function of doping concentration (referred to as a quenching curve) cannot be measured. Instead, we have compared quenching curves for bulk and nanophosphor Y_2O_3:Tb. When measured with PL, the bulk and nanophosphor specimens peak at 0.5 % and 1.5 % Ce concentrations respectively. The PL (or RL) does not continue to increase with Ce concentration as efficient energy transfer occurs among the Ce ions above a certain concentration and this increases the chances of energy transfer to a quenching center. In nanophosphors, energy transfer will be restricted to the crystallite and hence a higher Ce concentration is required before quenching effects become evident as compared to bulk crystals where energy transfer can take place throughout the entire crystal. The reduced quenching effects for n-oxyorthosilicates along with the ability to dope at higher Ce concentrations helps to increase the total light yield.

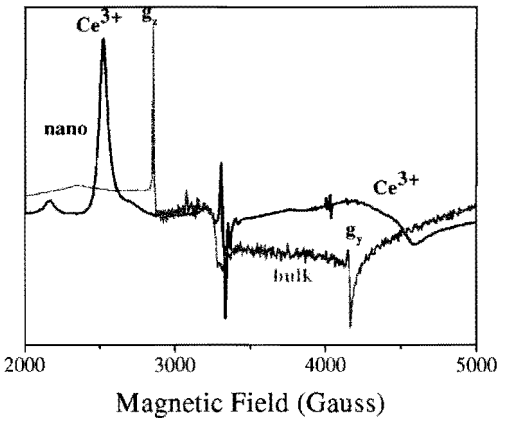

Figure 2 EPR spectra (measured at 10 K) of nano (black) and bulk (gray). The g_z and g_y Ce^{3+} resonances are marked. Note that the nano spectra has been multiplied by 6.

EPR measurements have revealed another possible decrease in quenching behavior for the nanophosphors. Fig. 2 shows EPR spectra for both bulk and nanophosphor LSO:Ce measured at temperatures below 10 K. The Ce lines can only be detected below approximately 50 K due to lifetime broadening of the lines above this temperature [12]. Although there is a slight shift in the g-values between the bulk and nanophosphor samples, of more significance is the broader linewidths displayed by the nanophosphor which are indicative of increased crystal disorder. In order to quantify the disorder, we studied the Orbach relationship for LSO and YSO (the Ce lines in GSO cannot be resolved). The Orbach process is a resonant two-phonon process involving the excited state of Ce^{3+} and relaxation from this state instead of the direct relaxation employed in the typical EPR process. The temperature-dependent linewidth of the Ce^{3+} EPR resonance in the Orbach process is indicative of the inhomogeneous broadening due to crystal disorder [12]. The linewidth for the g_z resonance was measured for LSO spectra taken at various temperatures and fit to the relationship:

$$lw=A+C*\Delta E^3*\exp(-E/k_bT) \quad (1)$$

where lw (Gauss) is the FWHM of the resonance, A (Gauss) is the inhomogeneous broadening due to lattice disorder, C is a constant, and ΔE (cm-1) is the energy splitting between the excited states. The energy splittings and crystal disorder for bulk and nanophosphor LSO and YSO are summarized in Table 1. Although there is no consistent variation in the energy splittings, the nanophosphor samples show over a tenfold increase in crystal disorder. The increase in crystal disorder is expected as a result of the SCS method and has large implications for the luminescence properties as resonance energy transfer is presumably less efficient and quenching processes are less effective.

(A) for bulk and nanophosphor samples derived from fitting the Orbach relationship (Eq. 1) to temperature-dependent EPR.

TL and OSL measurements have also shown that the concentration of trapping centers is reduced in nano-

Sample	ΔE (cm^{-1})	A (Gauss)
LSO Bulk	159±8	5.0±0.8
LSO Nano	153±9	81.8±1.5
YSO Bulk	143±4	5.8±0.5
YSO Nano	204±6	67.8±2.4

phosphor oxyorthosilicates. When normalized for differences in mass and dose, the bulk phosphors have TL and OSL intensities 2 and 3 orders of magnitude greater than nanophosphors respectively (Fig. 3). Since the PL measurements do not show this trend, it can be assumed that the reduced TL and OSL signals are due to reduced concentrations of electron trapping centers. Fewer electron trapping centers imply reduced competition for electron-hole recombination during the RL process and may help explain the increased light yield as measured by RL.

4 Aluminium oxide

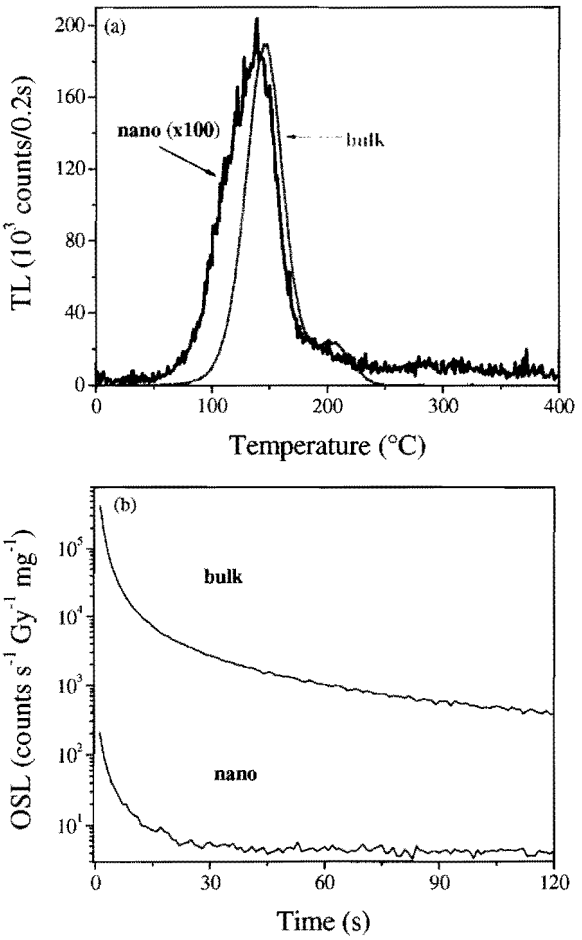

Figure 3 (a) TL and (b) OSL for bulk and nanophosphor YSO.

Al_2O_3:C has been successfully employed as a personal OSL dosimeter as it is highly sensitive to ionizing radiation and the signal is stable over the time period of interest [13]. Although this material has been developed for the commercial Luxel™ system, the materials are still produced by crystal growth techniques [13]. If we can produce nanophosphor Al_2O_3 samples by the SCS method that are nominally as bright as bulk Al_2O_3:C samples, it may be advantageous to produce nanophosphor Al_2O_3 samples for purely practical reasons.

In order to investigate this possibility, we have used the SCS method to produce nanophosphor Al_2O_3 samples using aluminium hydroxide as a starting material, and no doping of the nanophosphors was attempted. We also used three different fuels (Glycine, Urea, and HMT) in both stoichiometric and fuel-rich mixtures. Therefore, we produced six different Al_2O_3 samples. After combustion, the samples were annealed at 900 ^{0}C (as opposed to 1000 ^{0}C) for 1 hour in air to remove any excess fuel and nitrates.

4.1 Nanophosphor Al_2O_3 structure

XRD results revealed that only the urea fuel produced phase-pure nanophosphor Al_2O_3. Both urea-produced samples (stoichiometric and fuel-rich) produced XRD patterns that of a hexagonal close-packed (HCP) structure that is consistent with α-Al_2O_3. It is important to note that commercially available Al_2O_3:C also shows a phase pure α-Al_2O_3 [14]. Nanophosphor samples made with glycine and HMT fuels did not show clear XRD patterns and probably represent mixed-phase samples.

4.2 TL and OSL dosimetric properties

As the purpose of studying nanophosphor Al_2O_3 samples is to develop passive dosimetry materials, we tested the basic dosimetric properties of the produced nanophosphor materials.

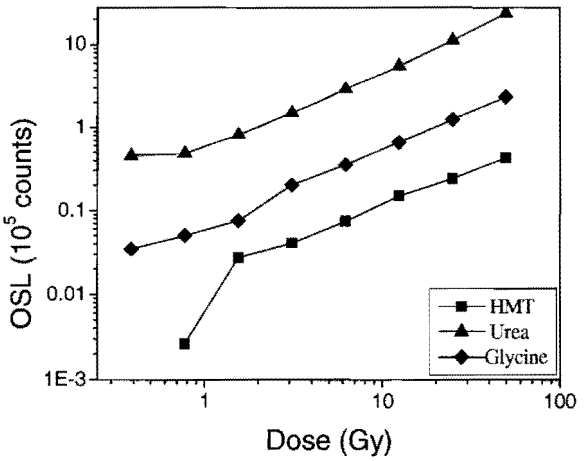

Figure 4 OSL dose response curves for Al_2O_3 nanophosphors produced using the three fuels indicated (stoichiometric concentrations).

The TL signals from nanophosphors made using urea and glycine were easily bleached by exposure to blue light (470 nm +/- 20 nm) for 500 s. This is an important property for OSL dosimetry which has distinct advantages as compared to TL dosimetry. The HMT produced samples, though, showed a significant residual TL signal under the same bleaching conditions. The residual TL signal may be due to retrapping of electrons as the TL peak position shifts to lower temperature with increasing radiation dose implying non first-order kinetics and substantial retrapping. The urea and glycine produced samples, on the other hand, both show first-order kinetics along with favourable bleaching characteristics.

The radiation dose response curves yield different results. The dose response of the nanophosphors was only monitored over a short range by both TL and OSL, and the minimum detectable dose appears to be relatively high when compared to commercially available Al_2O_3:C. Yet, more importantly, nanophosphor samples produced with urea (using both stoichiometric and fuel-rich concentrations) have a linear dose response over the measured range and show no signs of saturation. However, both glycine and HMT fuels produced nanophosphors with non-linear dose responses even over the limited range of these measurements (Fig. 4).

4.3 Comparison with bulk Al_2O_3:C

Even if nanophosphor Al_2O_3 samples do have the basic dosimetric properties required for OSL and TL dosimetry, nanophosphor samples will probably be of limited use if their properties and light yield differ significantly from bulk Al_2O_3:C. In order to directly compare the TL and OSL signals from nanophosphor Al_2O_3 and bulk Al_2O_3:C, we used a $^{90}Sr/^{90}Y$ radiation source placed at a greater distance from the sample position that delivered approximately 0.014 Gy/s. The lower dose rate enabled us to measure OSL and TL from Al_2O_3:C without

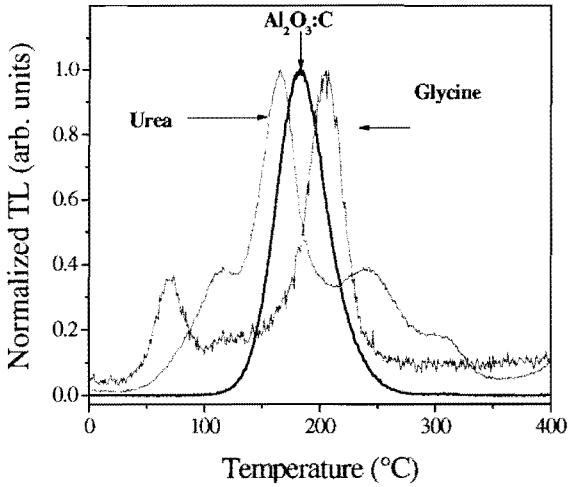

Figure 5 Normalized TL curves for bulk Al_2O_3:C and nanophosphors produced with two different fuels as labeled.

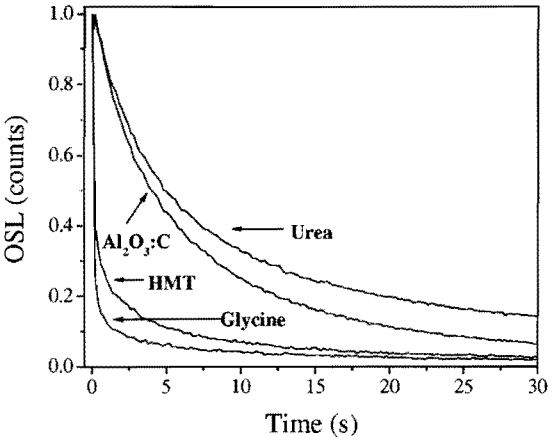

Figure 6 Normalized OSL curves for bulk Al_2O_3:C and nanophosphors produced with two different fuels as labeled.

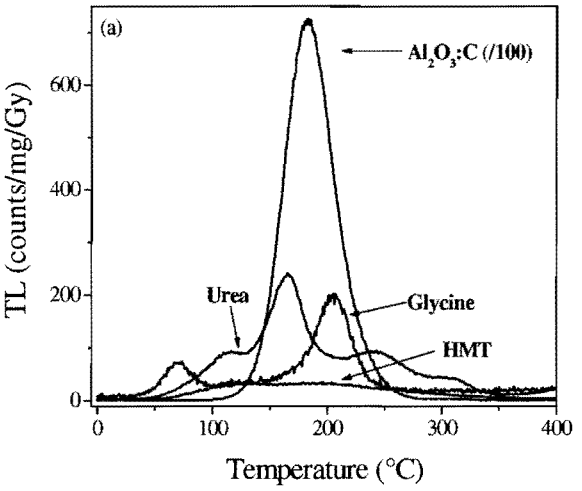

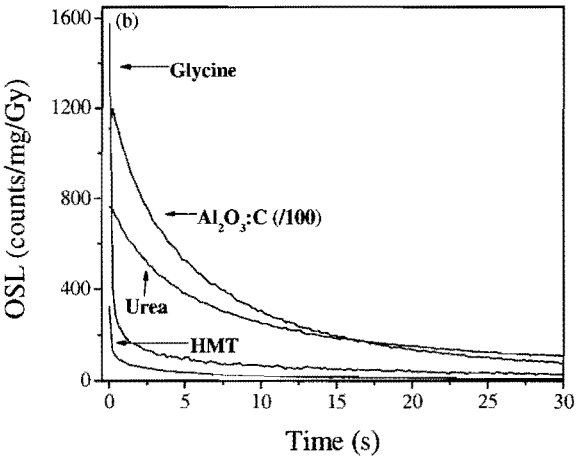

Figure 7 Mass and dose normalized (a) TL and (b) OSL curves for bulk Al_2O_3:C and nanophosphors produced with the indicated fuels.

saturating the PMT.

The normalized TL curves of bulk and nanophosphor samples in Fig. 5 show that urea and glycine produced nanophosphors are similar to Al_2O_3:C in that all three curves have a dominant peak near 200 ^{0}C. However, the nanophosphor samples also show significant peaks both above and below the main TL peak whereas Al_2O_3:C does not. This could mean that the SCS method produces more types of defects (in significant concentrations) as compared to crystal growth techniques.

Although normalized TL curves would suggest that two fuels produce nanophosphors with properties similar to Al_2O_3:C, normalized OSL curves show a different trend. Both glycine and HMT produced nanophosphors show rapid OSL decay while urea produced nanophosphors and bulk Al_2O_3:C samples both show much slower OSL decays (Fig. 6) . These results are not surprising since XRD showed that only urea produced nanophosphors have the same crystal structure and phase as Al_2O_3:C. Although faster OSL decays are preferred in many circumstances, the slow decay of Al_2O_3:C (and urea produced nanophosphor Al_2O_3) makes using the pulsed OSL technique practical and greatly increases the usefulness of Al_2O_3:C [15].

Direct comparison of the TL and OSL intensities for nanophosphor and bulk samples reveal that bulk Al_2O_3:C is considerably brighter than the SCS produced Al_2O_3 nanophosphors. Both TL and OSL curves (Fig. 7) have been normalized by mass and radiation dose to give luminescence intensity per unit mass per unit dose. The urea produced samples yield light intensities most comparable to Al_2O_3:C, but the initial intensities (taken from Fig. 7) and the integrated intensities given in Table 2 are approximately 100 times smaller for the SCS produced nanophosphors than for bulk Al_2O_3:C.

Table 2 TL and OSL integrated intensities for Al_2O_3:C and nanophosphors produced by indicated fuels.

Sample	TL	OSL
Al_2O_3:C	4.6e6	6.9e6
Glycine	1.7e4	3.1e4
Urea	2.5e4	8.0e4
HMT	6.9e3	9.7e3

5 Conclusions

We have briefly examined the structural and optical properties of two different classes of nanostructured materials.

Light yield from the nanophosphor oxyorthosilicates is of the same magnitude as the bulk counterparts due at least partially to multiple reasons. PL and PLE present red shift and greater Stokes shift in relation to bulk materials (for LSO and YSO) and hence reduced self-absorption. Quenching effects are also reduced in the nanophosphor materials due to less efficient energy transfer as evidence by PL quenching curves and the Orbach mechanism measured by EPR. Finally, TL and OSL measurements showed that the nanophosphor samples have lower concentrations of trapping centres which probably increase RL signals.

Results from attempts to produce bright Al_2O_3 dosimetry materials by the SCS method were more mixed. Although the amount of fuel (i.e., stoichiometric vs. fuel-rich) has been important in synthesizing other nanophosphors, this factor seemed to make little difference in the performance of n-Al_2O_3 samples. Both urea and glycine produced nanophosphors displayed optically bleachable TL signals and first-order kinetics, but only urea produced samples yielded linear dose response curves. However, all of the SCS produced n-Al_2O_3 samples were orders of magnitude less bright than bulk Al_2O_3:C and hence their practical applications would be limited. The most likely explanation for the weak TL and OSL signals is the lack of doping (e.g., with C) that results in lower concentrations of oxygen vacancies.

Acknowledgements This work was supported in part by DOE, Office of Basic Energy Sciences.

References

[1] H. Doumanidis, Nanotech. **13**, 248 (2002).
[2] H. Chander, Mat. Sci. Eng. R **49**, 113 (2005).
[3] P. Dorenbos, Nucl. Instrum. Meth. Phys. Res. A **486**, 208 (2002).
[4] J.J. Kingsley and K. C. Patil, Mat. Lett. **6**, 427 (1988).
[5] L. Bøtter-Jensen, E. Bulur, G.AT. Duller, and A. S. Murray, Radiat. Meas. **32**, 523, 2000.
[6] H. Suzuki, T. A. Tombrello, C. L. Melcher, and J. S. Schweitzer, Nucl. Inst. Meth. Phys. Res. A **320**, 263 (1992).
[7] C. Granquist, L. Kisyh, and W. Marlow (eds), Gas Phase Nanoparticle Synthesis (Kluwer, Dordrecht, The Netherlands, 2004) ch. 3, sec. 4.4.
[8] L. G. Jacobsohn, B. L. Bennett, R. E. Muenchausen, J. F. Smith, and D. W. Cooke, J. Solid State Chem., submitted for publication.
[9] D. W. Cooke, J. K. Lee, B. L. Bennett, J. R. Groves, L. G. Jacobsohn, E. A. McKigney, R. E., Muenchausen, M. Nastasi, K. E. Sickafus, M. Tang, and J. Valdez, Appl. Phys. Lett. **88**, 103108 (2006).
[10]R. E. Muenchausen, E. A. McKigney, L. G. Jacobsohn, M. W. Blair, B. L. Bennett, and D. W. Cooke, IEEE Trans. Nuc. Sci. **55**, 1532 (2008).
[11]D. W. Cooke, K. J. McClellan, B. L. Bennett, J. M. Roper, M. T. Whittaker, R. E. Muenchausen, and R. C. Sze, J. Appl. Phys., **88**, 7360 (2000).
[12]L. Pidol, O. Guillot-Noël, A. Kahn-Harari, B. Viana, D. Pelenc, and D. Gourier, J. Phys. Chem. Solids **67**, 643 (2006).
[13]L. Bøtter-Jensen, S. W. S. McKeever, and A. G. Wintle, Optically Stimulated Luminescence Dosimetry (Elsevier, Amsterdam, 2003), ch. 4.
[14]M.S. Akselrod, V. S. Kortov, E. A. Gorelova, Radiat. Prot. Dosim. **47**, 159 (1993).

[15]S.W.S. McKeever, M.W. Blair, E. Bulur, R. Gaza, R. Gaza, R. Kalchgruber, D. M. Klein, and E. G. Yukihara, Radiat. Prot. Dosim. **109**, 269 (2004).